Cell Reports, Volume *42*

Supplemental information

A trypanosome-derived immunotherapeutics platform elicits potent high-affinity antibodies, negating the effects of the synthetic opioid fentanyl

Gianna Triller, Evi P. Vlachou, Hamidreza Hashemi, Monique van Straaten, Johan P. Zeelen, Yosip Kelemen, Carly Baehr, Cheryl L. Marker, Sandra Ruf, Anna Svirina, Monica Chandra, Katharina Urban, Anastasia Gkeka, Sebastian Kruse, Andreas Baumann, Aubry K. Miller, Marc Bartel, Marco Pravetoni, C. Erec Stebbins, F. Nina Papavasiliou, and Joseph P. Verdi

Suppl. Figure 1. Synthesis of fen-sort and fen-G4 (related to Figure 2)

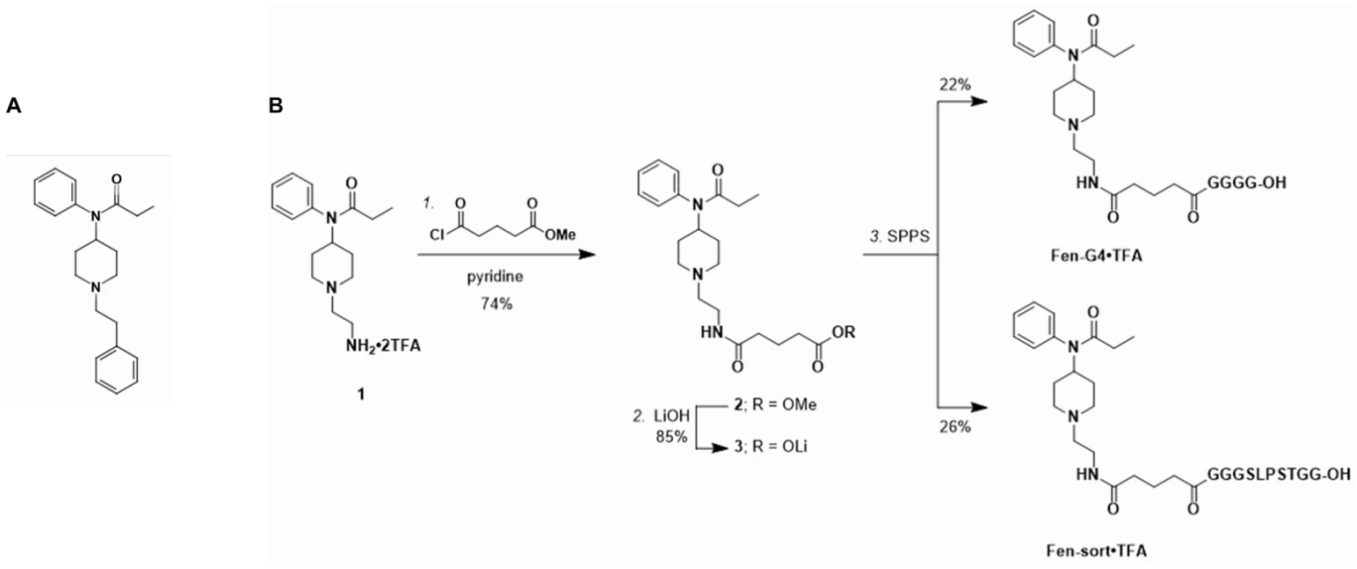

A. Chemical structure of the fentanyl molecule. B. Synthesis of the fentanyl derivatives used in this study. Reagents and conditions: 1. glutaric acid monomethyl ester chloride (1.0 equiv), pyridine (6.0 equiv), CH_2Cl_2, 0 °C to rt, 16 h, 74%; 2. LiOH (3 equiv), MeOH/H_2O (4:1), rt, 22 h, 85%; 3. Solid-phase peptide synthesis using an Fmoc protection strategy provided fen-G4 (22%) and fen-sort (26%) as trifluoroacetate salts (see experimental section for reaction details). Fen-sort was used to generate Fent-VASTs, while fen-G4 was used to generate fent-BSA for ELISA coating and for some of the co-crystallization studies. Both the sortaggable and poly-glycine versions of fentanyl are missing the extended aromatic ring at the bottom of the molecule. Amino acids are displayed using their single letter codes in black text. Note that this is a modified version of a previously published synthesis[1,2].

Suppl. Figure 2. Vaccination material, schedule, and boost-timing-dependent antibody titers (related to Figure 2)

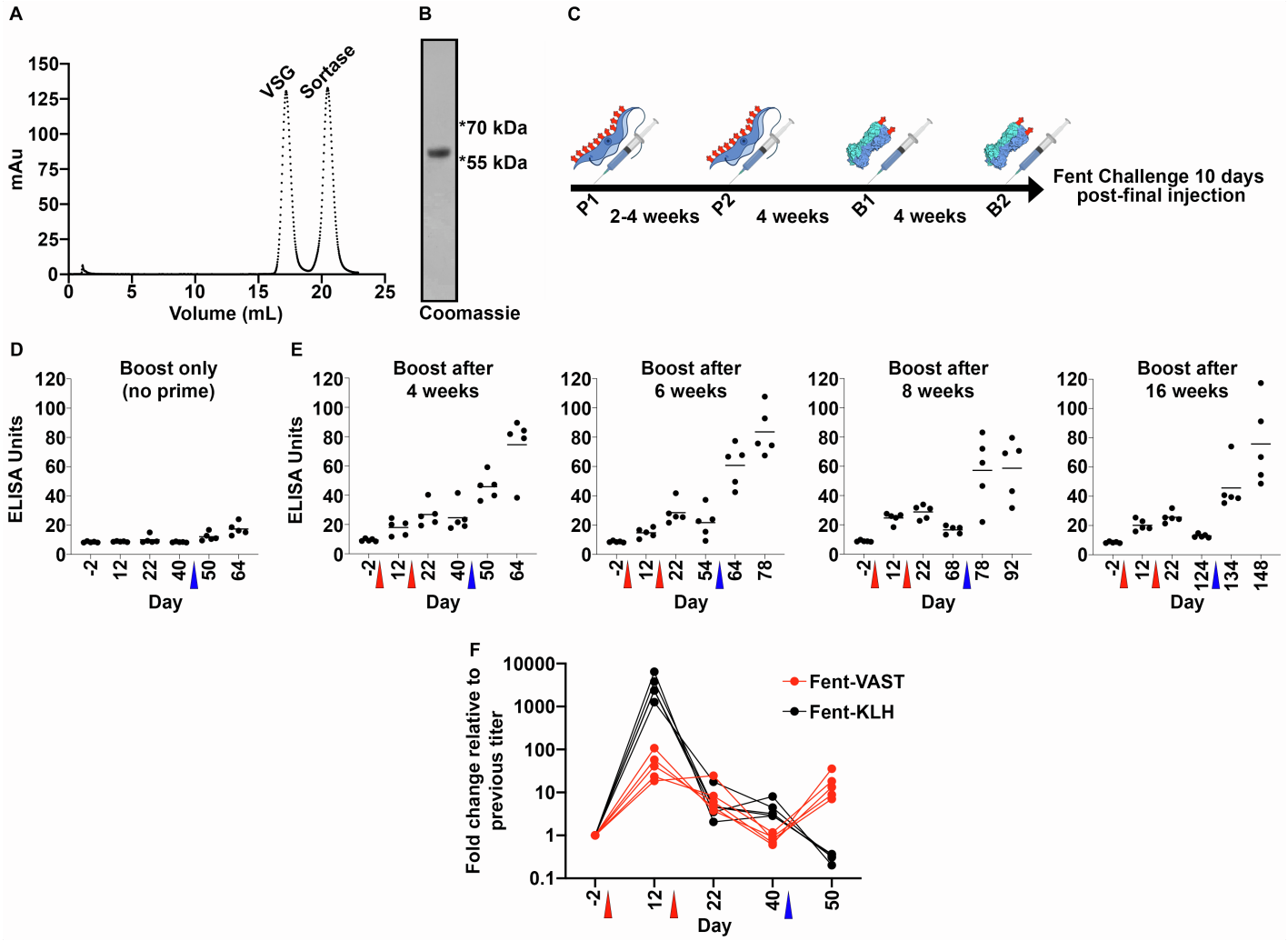

A. Gel filtration chromatogram (from a Superose 6 increase 10/300 column; Cytiva) showing the re-purification of VSG after a sortagging reaction. The Y-axis depicts the absorbance at 280 nM, represented as milli-absorbance units (mAu). B. Coomassie-stained SDS PAGE separation of the VSG peak from (A). VSG, existing as a >55 kDa monomer, is the only observable protein in the eluted sample. C. The general vaccination schedule according to which mice represented by Figures 2 and 3 were injected with Fent-VASTs, with the time intervals between each vaccination denoted between each injection day. P1 and P2; the two prime injections were composed of UV-irradiated fentanyl-coated *T. brucei* surface coats. B1 and B2; the two boost injections were composed of soluble Srt-VSG3 conjugated to fen-sort. Fentanyl challenge studies were always conducted 10 days post-B2. D. Anti-fentanyl antibody titers in mice immunized once (blue arrowhead) with soluble fen-sort-conjugated Srt-VSG3. The ELISA units shown in D and E are normalized to the signal generated by a control antibody (an anti-fentanyl mAb) to ensure comparability from graph to graph. Means are shown. E. Anti-fentanyl antibody titers in mice immunized with modified schedules as indicated above each graph. The prime injections were 2 weeks apart (at days 0 and 14), and are marked by red arrowheads. The mice were then boosted one time: 4, 6, 8, or 16 weeks after the second prime injection. The boost injections are marked by the blue arrowheads. F. Antibody titer jumps after each injection of Fent-KLH (adjuvanted with alum) or Fent-VAST in 5 mice per group. Each trajectory indicates the titer jumps in one individual mouse. Red arrowheads indicate the timing of the prime injections, while the blue arrowhead indicates the timing of the boost. The mathematical comparisons from day to day were made based on the calculated midpoint titer at each individual bleed day divided by the midpoint titer from the previous bleed day, although the pre-bleed (day -2) was assigned to 1 for all mice to facilitate the generation of an informative graph.

Suppl. Figure 3. Behavioral assays following active immunization (related to Figure 3)

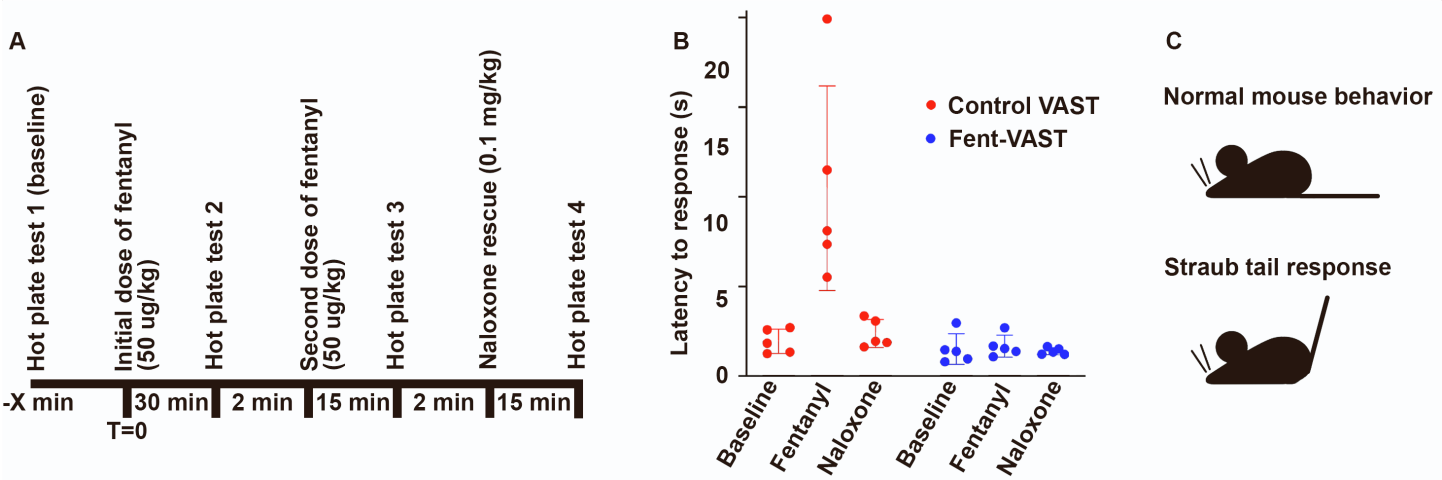

A. Experimental setup of the hot plate assay is shown. B. Analgesic activity was tested by using the hot plate assay as described in A. Fentanyl's effect on hot plate antinociception was tested in mice immunized with control-VAST and in mice immunized with Fent-VAST. The effect of 100 µg/kg fentanyl is shown as time-until-movement (latency) in seconds. Means ± standard deviation of 5 mice are shown, with circles representing the individual mice. Red shows mice immunized with control-VAST and blue mice immunized with Fent-VAST. C. Straub-Tail reaction and the position of the tail of normal mice and mice intoxicated with fentanyl is shown.

Suppl. Figure 4. Isolation and characterization of memory B cells (related to Figure 4)

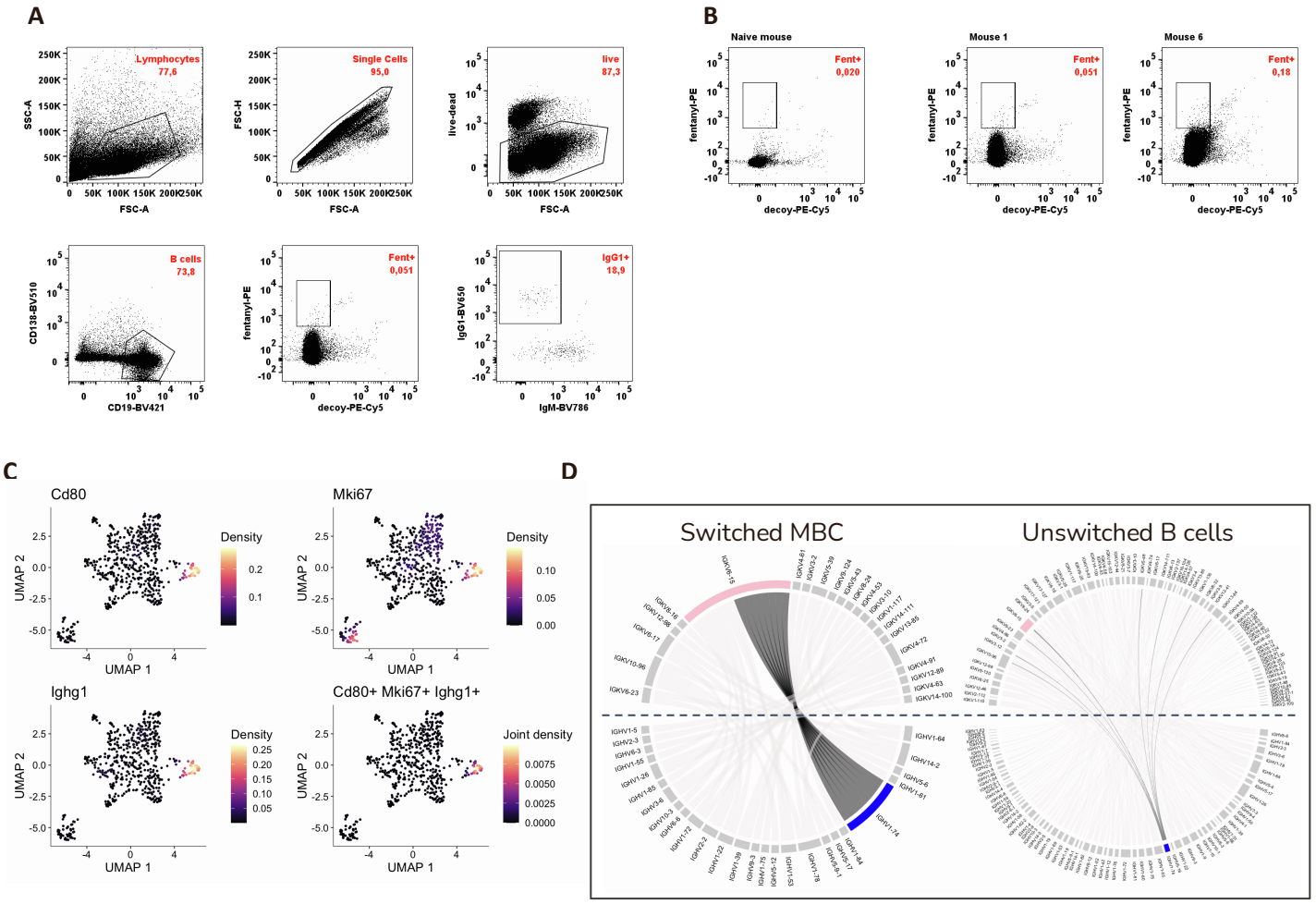

A. Gating strategy for sorting fentanyl-specific B cells from mice immunized as indicated in Supp. Figure 2C. Splenocytes from two mice were stained with a live/dead marker, several B cell markers (CD19-BV421 and CD138-BV510), SA-BSA-PE-AF647 (decoy), and fentanyl-PE as bait. Fentanyl-PE single positive cells were sorted into 384 well plates and processed as described in the methods section. B. Sort gates for splenocytes pre-gated as shown in A for a naïve mouse and two immunized mice. The percentage of fentanyl-binding B cells in the total B cell pool is shown in red. C. UMAP visualizing the expression density of the Cd80, Mki67 and Ighg1 genes and the joint expression is shown. Each UMAP depicts the kernel density estimates of each of the selected genes, using the normalized gene expression as an input. The joint expression is calculated by multiplying the kernel density estimates from all 3 genes. Beige indicates a relatively high simultaneous expression pattern, while purple indicates low simultaneous expression. D. Circos plots show the switched memory B cell variable region repertoire compared to the non-switched B cell repertoire, for both mice combined. The expanded heavy (in blue - IGHV1-74) and light (in pink - IGKV6-15) variable regions are highlighted. In dark gray we show the pairing of the IGHV1-74 variable region of the heavy chain with the corresponding variable region of the light chains. In the switched memory B cell population (Switched MBCs) all the cells expressing a BCR with an IGHV1-74 variable region are paired with a IGKV6-15 light variable region, showing the expansion of this gene usage inside the population. This is not the case for the non-switched cells that belong to the other B cell subpopulations (right panel). There is only one cell expressing a BCR containing both an IGHV1-74 and IGKV6-15.

Suppl. Figure 5. Mass spectrometry and behavioral assays following passive immunizations (related to Figure 5)

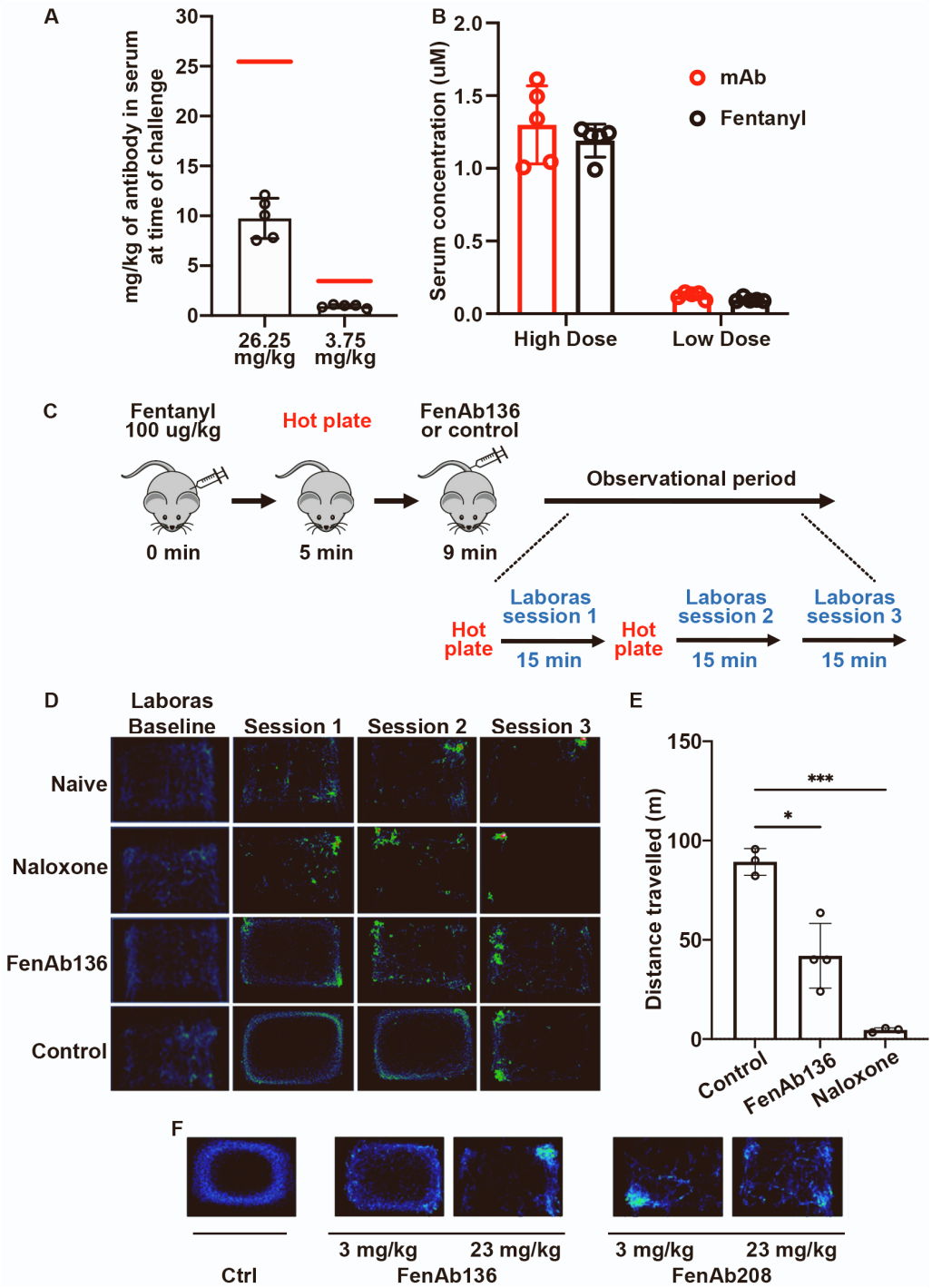

A. The amount of serum-circulating antibody at the time of fentanyl challenge post-passive therapy (see Figure 5E and F) was analyzed by western blot and plotted here. The red lines indicate the hypothetical antibody level if 100% of the injected antibody was present in the serum, revealing the approximately 2-3-fold lower-than-maximum levels of antibody in the serum at time of challenge. Means ± SD of 5 mice per group are shown. B. The molar serum concentrations of anti-fentanyl IgG and fentanyl are plotted. The values suggest that approximately 95-98% of the serum-circulating antibody is able to capture fentanyl after drug injection. Means ± SD of 5 mice per group are shown. C. A graphical description of the "rescue experiment" is shown. Fentanyl (100 µg/kg) is injected prior to either control, naloxone, or FenAb136 administration (delivered i.v.). FenAb136 was delivered at 26 mg/kg. Hot plate assays were executed at the indicated time points (with the data shown in Figure 5G), while 15-min long LABORAS recording sessions were spaced as indicated. Baseline measurements

for both the hot plate and LABORAS readings were taken prior to fentanyl injection (not shown in the graphic). D. LABORAS heat maps recorded during the experiment described in C. The maps are projections of 15 minutes' worth of movement of individual mice. Mice displaying normal mouse behavior (see the naïve mouse – an individual that was not injected with anything) tend to spend the majority of their time in one corner of the cage, showing a reduction in locomotion as time passes (as they acclimatize to the cage). Fentanyl intoxicated mice move around the periphery of their cage (see control sessions 1 and 2) until the effect of the drug begins to wear off (see control session 3). E. The summation of total distance traveled (in meters) across all three post-treatment LABORAS sessions is shown. These data are collected by the movement tracking software. Means ± SD of >3 mice per group are shown. *$p<0.05$, ***$p<0.001$; Dunnett's multiple comparisons test following one-way ANOVA. F. LABORAS movement tracking maps collected from the mice represented in Figure 5H. A 15-min recording taken immediately after the 5-min timepoint in Figure 5H, thus prior to the 20-min time point, is projected.

Suppl. Figure 6. Purification and crystallography of recombinant antibody-fentanyl complexes (related to Figure 6)

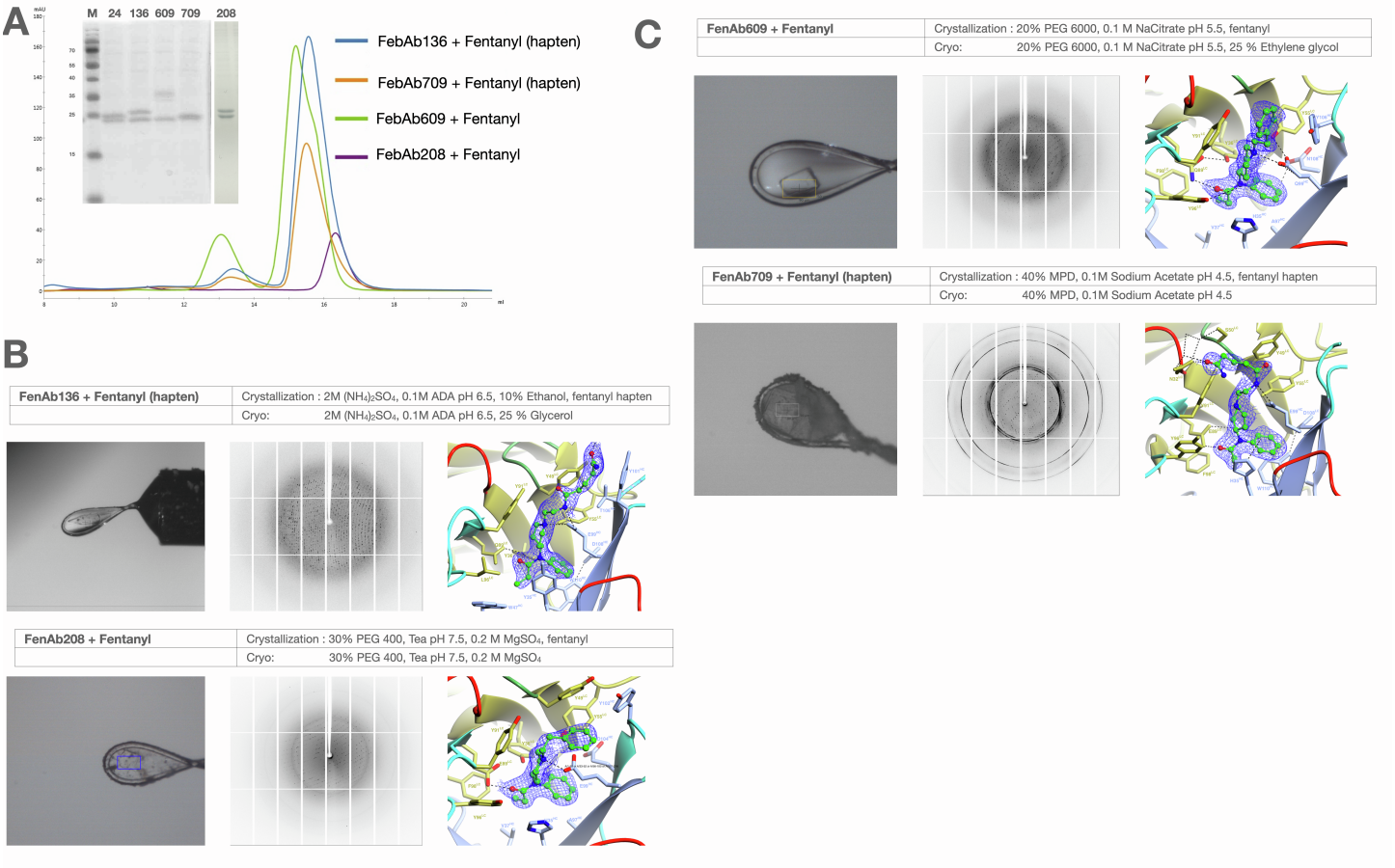

A. Superimposed size exclusion chromatograms characterizing the final material used in crystallization experiments are shown. Elution volumes are depicted along with absorbance units at 280 nm. The individual chromatograms are colored for each Fab and ligand as indicated in the key. An SDS gel stained with Coomassie blue shows the contents of the peak fractions (M indicates molecular weight markers with several of those bands shown on the left side of the gel in kDa, whereas the gel lanes are labeled above for the antibody number). B-C. Three panels are shown for each antibody-ligand complex with the crystallization and cooling conditions (labeled): cryo-cooled crystal mounted in loop at the synchrotron during data collection, sample diffraction, and 2Fo-Fc electron density map focused on the ligand contoured at 1 sigma from final refinements. The protein and ligand are illustrated similar to Figure 6C.

Suppl. Table 1. Data collection and refinement statistics.

	FenAb136	FenAb208	FenAb609	FenAb709
Wavelength (Å)	1.0	1.0	1.0	1.0
Resolution range (Å)	54.52 - 2.07 (2.14 - 2.07)	48.49 - 1.92 (1.99 - 1.92)	45.19 - 1.7 (1.76 - 1.70)	55.32 - 2.32 (2.40 - 2.32)
Space group	C121	P 41	P 21 21 21	C 2 2 21
Unit cell Dimensions (Å)	182.98 105.84 172.77 90 112.24 90	153.34 153.34 45.99 90 90 90	77.27 111.41 114.81 90 90 90	75.19 138.69 101.07 90 90 90
Total reflections	361101 (35110)	414373 (39287)	727900 (70440)	243094 (25540)
Unique reflections	181970 (17881)	82358 (8154)	109391 (10846)	22297 (2274)
Multiplicity	2.0 (2.0)	5.0 (4.8)	6.7 (6.5)	10.9 (11.2)
Completeness (%)	97.51 (96.49)	99.85 (99.88)	99.89 (99.71)	94.77 (100.00)
Mean I/sigma(I)	7.29 (1.20)	11.69 (1.05)	11.31 (0.95)	16.19 (7.30)
Wilson B-factor (Å^2)	35.64	33.63	25.77	25.34
R-merge	0.0637 (0.5982)	0.08342 (1.312)	0.09267 (1.943)	0.09728 (0.2856)
R-meas	0.09008 (0.8459)	0.09322 (1.475)	0.1006 (2.111)	0.1021 (0.2991)
R-pim	0.0637 (0.5982)	0.04106 (0.6656)	0.03887 (0.819)	0.03055 (0.08823)
CC1/2	0.987 (0.584)	0.999 (0.577)	0.999 (0.608)	0.998 (0.978)
CC*	0.997 (0.859)	1 (0.856)	1 (0.87)	0.999 (0.995)
Reflections used in refinement	180911 (17746)	82332 (8148)	109323 (10826)	22035 (2274)
Reflections used for R-free	1986 (185)	4117 (408)	5470 (542)	1110 (149)
R-work	0.2424 (0.3486)	0.1960 (0.3754)	0.2015 (0.4464)	0.2096 (0.2261)
R-free	0.2816 (0.3953)	0.2299 (0.3960)	0.2302 (0.4786)	0.2446 (0.2859)
CC(work)	0.921 (0.540)	0.966 (0.788)	0.962 (0.810)	0.932 (0.896)
CC(free)	0.904 (0.536)	0.960 (0.720)	0.942 (0.808)	0.910 (0.784)
Number of non-hydrogen atoms	21106	7011	7371	3469
macromolecules	19606	6550	6822	3180
ligands	172	50	50	28
solvent	1328	411	499	261
Protein residues	2558	852	855	415
RMS(bonds) (Å)	0.002	0.011	0.010	0.004
RMS(angles) (Å)	0.52	1.14	1.06	0.72
Ramachandran favored (%)	97.94	98.21	98.46	97.27
Ramachandran allowed (%)	2.06	1.67	1.54	2.73
Ramachandran outliers (%)	0.00	0.12	0.00	0.00
Rotamer outliers (%)	1.22	0.93	0.89	3.57
Clashscore	2.86	3.09	1.71	3.68
Average B-factor (Å^2)	45.82	43.26	37.22	32.42
macromolecules	45.85	43.22	37.20	32.69
ligands	46.12	41.48	30.41	27.19
solvent	45.40	44.17	38.13	29.67
Number of TLS groups	50	18	14	8
Statistics for the highest-resolution shell are shown in parentheses.				

Suppl. Table 2. Oligo list

Primer source	Primer name	Primer sequence	Used for	Reference
Eurofins	H1_fw	AGTAGCAACTGCAACCGG	Amplification of FenAb136 heavy chain and addition of NEBuilder homology region for Fab vector construction	This manuscript
Eurofins	H0_rv	GTCGTTTTGGCTGAGGAGAC	Amplification of FenAb136, 609, 709, and 024 heavy chains and addition of NEBuilder homology region for Fab vector construction	This manuscript
Eurofins	H0_fw	GTCTCCTCAGCCAAAACGAC	Amplification of Fab heavy chain expression vector and addition of NEBuilder homology region for FenAb136 cloning	This manuscript
Eurofins	H1_rv	CGGTTGCAGTTGCTACTA	Amplification of Fab heavy chain expression vector and addition of NEBuilder homology region for FenAb136 cloning	This manuscript
Eurofins	k1_fw	GCAACCGGTGTACATTCAG	Amplification of FenAb136 light chain and addition of NEBuilder homology region for Fab vector construction	This manuscript
Eurofins	k0_rv	TCAGTTGTTCGGAGGAAGG	Amplification of FenAb136 light chain and addition of NEBuilder homology region for Fab vector construction	This manuscript
Eurofins	k0_fw	CCCTTCCTCCGAACAACTG	Amplification of Fab heavy and light chain expression vectors and addition of NEBuilder homology region for FenAb136, 609, 709, and 024 cloning	This manuscript
Eurofins	k1_rv	CTGAATGTACACCGGTTGC	Amplification of Fab light chain expression vector and addition of NEBuilder homology region for FenAb136 cloning	This manuscript
Eurofins	H2_fw	TCCAACTGCAGCAGCCTGG	Amplification of FenAb609, 709, and 024 heavy chains and addition of NEBuilder homology region for Fab vector construction	This manuscript
Eurofins	H2_rv	CAGGCTGCTGCAGTTGGAC	Amplification of Fab heavy chain expression vector and addition of NEBuilder homology region	This manuscript
Eurofins	I-H/L_fw	CATGGGATGGTCATGTATC	Amplification of FenAb208 heavy and light chain and addition of NEBuilder homology region for Fab vector construction	This manuscript
Eurofins	I208H_rv	TCTTAGCAGAGGAGACTGTGAGAGTGGTG	Amplification of FenAb208 heavy chain and addition of NEBuilder homology region for Fab vector construction	This manuscript
Eurofins	V-H/L_fw	CTCACAGTCTCCTCTGCTAAGACCACTGCG	Amplification of Fab heavy and light chain expression vector and addition of NEBuilder homology region for FenAb208 cloning	This manuscript
Eurofins	V208H_rv	GATACATGACCATCCCATG	Amplification of Fab heavy chain expression vector and addition of NEBuilder homology region for FenAb208 cloning	This manuscript
Eurofins	I208k_rv	GCATCAGCCCGTTTTATTTCCAGCTTGGTCCC	Amplification of FenAb208 light chain and addition of NEBuilder homology region for Fab vector construction	This manuscript
Eurofins	V208k_rv	TGGAAATAAAACGGGCTGATGCTGCAC	Amplification of Fab light chain expression vector and addition of NEBuilder homology region for FenAb208 cloning	This manuscript
Eurofins	024_N93S_fw	CTGTCAGCAATACAACAGCTATCCTCTCACGTTCG	Site-directed mutagenesis to create FenAb024 kappa chain from the FenAb136 kappa chain template	This manuscript
Eurofins	024_Y53H_fw	GATTTACTCGGCATCCCACCGGTACAGTGG	Site-directed mutagenesis to create FenAb024 kappa chain from a modified FenAb136 kappa chain template	This manuscript
Eurofins	609_L96Y-A100G_fw	CAACAACTATCCTTACACGTTCGGTGGTGGGACCAAGCTG	Site-directed mutagenesis to create FenAb609 kappa chain from the FenAb136 kappa chain template	This manuscript
Eurofins	609_L106I_fw	GGGACCAAGCTGGAGATTAAACGGGCTGATGCCG	Site-directed mutagenesis to create FenAb609 kappa chain from a modified FenAb136 kappa chain template	This manuscript
Eurofins	609_N93T_fw	CTGTCAGCAATACAACACCTATCCTTACACGTTCGG	Site-directed mutagenesis to create FenAb609 kappa chain from a modified FenAb136 kappa chain template	This manuscript

Eurofins	709_Y86-95F_fw	CTTGGCAGAGTTTTTCTGTCAGCAATACAACAACTTTCCTCTCACG	Site-directed mutagenesis to create FenAb709 kappa chain from the FenAb136 kappa chain template	This manuscript
Eurofins	709_L96Y-A100G_fw	CAACAACTTTCCTTACACGTTCGGTGGTGGGACCAAGCTG	Site-directed mutagenesis to create FenAb709 kappa chain from a modified FenAb136 kappa chain template	This manuscript
Eurofins	709_K103Q-L106M_fw	GTGGTGGGACCCAGCTGGAGATGAAACGGGCTG	Site-directed mutagenesis to create FenAb709 kappa chain from a modified FenAb136 kappa chain template	This manuscript
Eurofins	024_N93S_rv	CGAACGTGAGAGGATAGCTGTTGTATTGCTGACAG	Site-directed mutagenesis to create FenAb024 kappa chain from the FenAb136 kappa chain template	This manuscript
Eurofins	024_Y53H_rv	CCACTGTACCGGTGGGATGCCGAGTAAATC	Site-directed mutagenesis to create FenAb024 kappa chain from a modified FenAb136 kappa chain template	This manuscript
Eurofins	609_L96Y-A100G_rv	CAGCTTGGTCCCACCACCGAACGTGTAAGGATAGTTGTTG	Site-directed mutagenesis to create FenAb609 kappa chain from the FenAb136 kappa chain template	This manuscript
Eurofins	609_L106I_rv	CGGCATCAGCCCGTTTAATCTCCAGCTTGGTCCC	Site-directed mutagenesis to create FenAb609 kappa chain from a modified FenAb136 kappa chain template	This manuscript
Eurofins	609_N93T_rv	CCGAACGTGTAAGGATAGGTGTTGTATTGCTGACAG	Site-directed mutagenesis to create FenAb609 kappa chain from a modified FenAb136 kappa chain template	This manuscript
Eurofins	709_Y86-95F_rv	CGTGAGAGGAAAGTTGTTGTATTGCTGACAGAAAAACTCTGCCAAG	Site-directed mutagenesis to create FenAb709 kappa chain from the FenAb136 kappa chain template	This manuscript
Eurofins	709_L96Y-A100G_rv	CAGCTTGGTCCCACCACCGAACGTGTAAGGAAAGTTGTTG	Site-directed mutagenesis to create FenAb709 kappa chain from a modified FenAb136 kappa chain template	This manuscript
Eurofins	709_K103Q-L106M_rv	GGAGATGAAACGGGCTGAGCTGGGTCCCACCAC	Site-directed mutagenesis to create FenAb709 kappa chain from a modified FenAb136 kappa chain template	This manuscript
ThermoFisher	HeavyJ2Rev(609_709)	TGCGAAGTCGACGCTGAGGAGACTGTGAGAGG	To add a SalI restriction site to FenAb609 and FenAb709 heavy chain for restriction cloning into IgG vector	This manuscript
ThermoFisher	HeavyJ4Rev(136_024)	TGCGAAGTCGACGCTGAGGAGACGGTGACTGG	To add a SalI restriction site to FenAb024 and FenAb136 heavy chain for restriction cloning into IgG vector	This manuscript
ThermoFisher	HeavyFwd(709)	CTGCAACCGGTGTACATTCACAGGTCCAACTGAGCAACCTGG	To add an AgeI restriction site to FenAb709 heavy chain for restriction cloning into IgG vector	This manuscript
ThermoFisher	HeavyFwd(136_024_609)	CTGCAACCGGTGTACATTCACAGTGCCAACTGCAGCAGCCTGG	To add an AgeI restriction site to FenAb024, FenAb609, and FenAb709 heavy chain for restriction cloning into IgG vector	This manuscript
ThermoFisher	FentKappa FabEcoRI	TCGATTCACCATGGGATGGTCATGTATCAT	To add an EcoRI restriction site to FenAb136 light chain for restriction cloning into IgG vector	This manuscript
ThermoFisher	LightChain Rev	GCCACCGTACGTTTCAGCTCCAGCTTGGTC	To add a BsiWI s restriction ite to FenAb136 light chain for restriction cloning into IgG vector	This manuscript
ThermoFisher	Fab 2 IgG Fwd EcoRI Adder	GCCGCTGAATTCCACCATGGGATGGTCATGTATCAT	To add an EcoRI restriction site to FenAb024, FenAb609, and FenAb709 light chain for restriction cloning into IgG vector	This manuscript
ThermoFisher	024Fab 2 IgG Rev BsiWI Adder	CGGCATCCGTACGTTTCAGCTCCAGCTTGGTC	To add a BsiWI restriction site to FenAb024 light chain for restriction cloning into IgG vector	This manuscript

ThermoFisher	609Fab 2 IgG Rev BsiWI Adder	CGGCATCCGTACGTTTAATTTCCAGCTTGGTC	To add a BsiWI restriction site to FenAb609 light chain for restriction cloning into IgG vector	This manuscript
ThermoFisher	709Fab 2 IgG Rev BsiWI Adder	CGGCATCCGTACGTTTCATTTCCAGCTGGGTC	To add a BsiWI restriction site to FenAb709 light chain for restriction cloning into IgG vector	This manuscript
ThermoFisher	Oligo-dt	AAGCAGTGGTATCAACGCAGAGTACTTTTTTTTTTTTTTTTTTTTTTTTTVN	Anneals to all RNAs containing a poly-A tail. Used during RNAseq library preparation	Picelli, et al., Nature, 2014
Sigma	ISPCR	AAGCAGTGGTATCAACGCAGAGT	Used during RNAseq library preparation	Picelli, et al., Nature, 2014[3]
Sigma	TSO	AAGCAGTGGTATCAACGCAGAGTACATrGrG+G	Used during RNAseq library preparation	Picelli, et al., Nature, 2014[3]

References

1. Raleigh, M.D., Baruffaldi, F., Peterson, S.J., Le Naour, M., Harmon, T.M., Vigliaturo, J.R., Pentel, P.R., and Pravetoni, M. (2019). A Fentanyl Vaccine Alters Fentanyl Distribution and Protects against Fentanyl-Induced Effects in Mice and Rats. J. Pharmacol. Exp. Ther. *368*, 282–291. 10.1124/jpet.118.253674.

2. Robinson, C., Gradinati, V., Hamid, F., Baehr, C., Crouse, B., Averick, S., Kovaliov, M., Harris, D., Runyon, S., Baruffaldi, F., et al. (2020). Therapeutic and Prophylactic Vaccines to Counteract Fentanyl Use Disorders and Toxicity. J. Med. Chem. *63*, 14647–14667. 10.1021/acs.jmedchem.0c01042.

3. Picelli, S., Faridani, O.R., Björklund, A.K., Winberg, G., Sagasser, S., and Sandberg, R. (2014). Full-length RNA-seq from single cells using Smart-seq2. Nat. Protoc. *9*, 171–181. 10.1038/nprot.2014.006.